Ascaris suum NAD-Malic Enzyme Is Activated by L-Malate and Fumarate Binding to Separate Allosteric Sites†

William E. Karsten,§ June E. Pais,§,# G. S. Jagannatha Rao,‡ Ben G. Harris,‡ and Paul F. Cook*,§

Department of Chemistry and Biochemistry, University of Oklahoma, 620 Parrington Oval, Norman, Oklahoma 73019, and the Department of Microbiology and Immunology, University of North Texas Health Science Center at Fort Worth, 3500 Camp Bowie Boulevard, Fort Worth, Texas 76107-2699

Received January 17, 2003; Revised Manuscript Received May 16, 2003

ABSTRACT: The kinetic mechanism of activation of the mitochondrial NAD-malic enzyme from the parasitic roundworm *Ascaris suum* has been studied using a steady-state kinetic approach. The following conclusions are suggested. First, malate and fumarate increase the activity of the enzyme in both reaction directions as a result of binding to separate allosteric sites, i.e., sites that exist in addition to the active site. The binding of malate and fumarate is synergistic with the K_{act} decreasing by ≥10-fold at saturating concentrations of the other activator. Second, the presence of the activators decreases the K_m for pyruvate 3−4-fold, and the $K_{i\ Mn}$ ≥20-fold in the direction of reductive carboxylation; similar effects are obtained with fumarate in the direction of oxidative decarboxylation. The greatest effect of the activators is thus expressed at low reactant concentrations, i.e., physiologic concentrations of reactant, where activation of ≥15-fold is observed. A recent crystallographic structure of the human mitochondrial NAD malic enzyme [*13*] shows fumarate bound to an allosteric site. Site-directed mutagenesis was used to change R105, homologous to R91 in the fumarate activator site of the human enzyme, to alanine. The R105A mutant enzyme exhibits the same maximum rate and V/K_{NAD} as does the wild-type enzyme, but 7−8-fold decrease in both V/K_{malate} and V/K_{Mg}, indicating the importance of this residue in the activator site. In addition, neither fumarate nor malate activates the enzyme in either reaction direction. Finally, a change in K143 (a residue in a positive pocket adjacent to that which contains R105), to alanine results in an increase in the K_{act} for malate by about an order of magnitude such that it is now of the same magnitude as the K_m for malate. The K143A mutant enzyme also exhibits an increase in the K_{act} for fumarate (in the absence of malate) from 200 μM to about 25 mM.

The mitochondrial NAD-malic enzyme (E.C. 1.1.1.39) from *Ascaris suum* catalyzes the reversible divalent metal ion dependent oxidative decarboxylation of L-malate using NAD[1] to produce pyruvate, CO_2, and NADH. In the parasitic roundworm *A. suum*, 2 equivalents of L-malate are produced in the cytoplasm from 1 equivalent of glucose (*1*). The malate produced in the cytoplasm is transported into the mitochondrion where it undergoes a dismutation reaction (*2*). One equivalent of malate is acted upon by fumarase to produce fumarate, and the second malate equivalent is acted upon by malic enzyme to produce pyruvate, CO_2 and NADH (*1*, *3*−*4*). The NADH produced from the malic enzyme reaction is utilized by a flavo-protein-linked succinate dehydrogenase that reduces fumarate to succinate (*1*, *5*−*7*). Concomitant with the fumarate reduction is a site I phosphorylation of ADP to ATP, which is the major source of the anaerobic energy production for the worm. Regulation of malic enzyme activity by the worm would provide a means to achieve a balance between NADH and fumarate production and control energy production in the form of ATP.

Activation of the *A. suum* malic enzyme by fumarate was first reported by Landsperger and Harris (*8*). Fumarate appeared to activate the enzyme by decreasing the K_m value for malate. A more detailed characterization of fumarate activation revealed a decrease in the primary deuterium isotope effect in the presence of fumarate and led to the conclusion that fumarate decreases the off-rate constant for malate from the E:NAD:Mg:malate quaternary complex (*9*). At about the same time, it was shown that the substrate L-malate was also an activator as it could activate in the reverse, reductive carboxylation, reaction direction (*10*).

Malic enzyme is a homotetrameric protein consisting of a dimer of dimers (*11*−*12*). The crystal structure of the human mitochondrial NAD-dependent malic enzyme in complex with ATP, Mn^{2+}, tartronate, and fumarate revealed an allosteric binding site for fumarate (*13*). Fumarate is bound at the dimer interface with its carboxylate groups within hydrogen bonding distance to arginine 67 and arginine 91, respectively. It was also shown that mutation of R67 to serine

† This work was supported by grants to P.F.C. from the Oklahoma Center for Advancement of Science and Technology (HR99-081), the American Chemical Society (PRF 35894-AC4), and the National Science Foundation (MCB 0091207) and to B.G.H. from the National Institutes of Health (AI 24155; AI 41552) and the Robert A. Welch Foundation (BK 1309).

* Corresponding author: Tel 405-325-4581; FAX 405-325-7182. E-mail pcook@chemdept.chem.ou.edu.

§ University of Oklahoma.

‡ University of North Texas Health Science Center at Fort Worth.

Current address: Department of Biological Chemistry, University of Michigan, Ann Arbor, MI.

[1] Abbreviations: Hepes, *N*-(2-hydroxyethyl)piperazine-*N*′-2-ethanesulfonic acid; NAD, nicotinamide adenine dinucleotide; NADH, reduced nicotinamide adenine dinucleotide.

10.1021/bi034101w CCC: $25.00
Published on Web 07/25/2003

or R91 to threonine eliminated activation of the human enzyme by fumarate (*13*). The homologous residues in the *A. suum* enzyme are R81 and R105, respectively. A crystal structure of the *A. suum* malic enzyme cocrystalyzed with NADH, Mn^{2+}, and tartronate, an analogue of malate and fumarate, shows tartronate bound in a deep pocket at the dimer interface (*14*). In this structure, tartronate is bound with both of its carboxylates in hydrogen bonding distance to R105, one carboxylate and the hydroxyl group within hydrogen bonding distance to R81, and the other carboxylate within hydrogen bonding distance to Q78. Although tartronate is apparently bound at the fumarate activator site of the *Ascaris* malic enzyme, it interacts with the protein in a manner that differs from the way fumarate interacts with the human enzyme.

We report a detailed kinetic characterization of the activation of the *A. suum* malic enzyme by both L-malate and fumarate. Data are consistent with malate binding at the active site and an allosteric site, and with fumarate binding to a separate allosteric site. We also have prepared and characterized kinetically the R105A and K143A mutants of malic enzyme.

MATERIALS AND METHODS

Chemicals and Enzyme. The L-malate, pyruvate, fumarate, NAD, and NADH were purchased from SIGMA. The sodium bicarbonate was from Mallinckrodt, $MnSO_4$ was from Fisher Scientific and Hepes buffer was obtained from Amresco. The QuikChange site-directed mutagenesis kit was from Stratagene. The recombinant *A. suum* malic enzyme used in the studies has a 6-histidine N-terminal tail and was purified as described previously (*15*). All other chemicals and reagents used were obtained commercially and were of the highest purity available.

Enzyme Assays. Enzyme assays were done at 25 °C in 1-cm cuvettes using a Beckman DU640 UV−visible spectrophotometer. In the direction of oxidative decarboxylation of malate, malic enzyme activity was measured at varying concentrations of L-malate, divalent metal ion, and fumarate as indicated in the text. The NAD concentration was maintained at a concentration at least 10 times its K_m value, and reaction mixtures were maintained at pH 7, 100 mM Hepes. The reaction was followed at 340 nm to monitor the production of NADH (ϵ_{340}, 6220 M^{-1} cm^{-1}). Malic enzyme activity in the reductive carboxylation reaction direction typically contained variable concentrations of pyruvate, $MnSO_4$, CO_2 (added as bicarbonate and the CO_2 concentration calculated using the Henderson-Hasselbach equation), and NADH as indicated in the text. The reductive carboxylation reaction was monitored via the disappearance of NADH at 340 nm. Malic enzyme uses the uncomplexed form of the divalent metal ion and substrates (*16*), and corrections for chelate complexes were done using the following dissociation constants: Mg-malate, 25.1 mM, Mn-malate 5.37 mM, Mg-NAD 19.7 mM, Mn-NAD and Mn-NADH 12.9 mM, Mn-pyruvate 55 mM, $MnHCO_3$ 355 mM, Mn-fumarate 102 mM, and Mg-fumarate 350 mM (*17*, *18*). All substrate and activator concentrations reported in the text refer to the uncomplexed concentrations of substrates, activators, and divalent metal ion.

Fluorescence Titration. Fluorescence spectra were collected on an SLM 8100 spectrophotometer, using quartz cuvettes with an inner volume of 3 mL. The temperature of the reaction chamber was maintained at 25 °C during the experiments. The excitation wavelength was set to 280 nm, and emission spectra were measured between 320 and 600 nm at 2-nm intervals. A bandwidth of 5 nm was used for excitation and emission monochromators. Blank spectra, containing all components except enzyme, were collected and subtracted from sample spectra. The titration was carried out by sequentially adding a small volume (~5 μL) of malate from a concentrated stock solution. All spectra were collected at pH 7, 100 mM Hepes, with 100 μg/mL malic enzyme. All spectra were corrected for dilution resulting from the addition of malate.

Data Processing. Initial velocity data were fitted using BASIC versions of the FORTRAN programs devoped by Cleland (*19*). Saturation curves were fitted using eq 1

$$v = VA/(K_a + A) \quad (1)$$

Initial velocity data conforming to an equilibrium ordered or sequential kinetic mechanism were fitted using eqs 2 and 3, respectively.

$$v = VAB/(K_{ia}K_b + K_bA + AB) \quad (2)$$

$$v = VAB/(K_{ia}K_b + K_aB + K_bA + AB) \quad (3)$$

In eq 1−3, v is initial velocity, A and B are substrate concentrations, V is maximum velocity, K_{ia} is the dissociation constant for A; K_a and K_b are Michaelis constants for A and B.

R105A Mutant. The R105A and K143A mutants of malic enzyme were made according to the manufacturer's recommendations in the QuikChange site-directed mutagenesis kit. The template was the *A. suum* malic enzyme gene in the pQE30 or pQE32 expression vector from Qiagen. The R105A mutation was made using the forward primer 5′-GGATGGCCTTCAGGATGCTAATGAGAAGCTCTTCTATCG-3′ and the reverse primer 5′-CGATAGAAGAGCTTCTCATTAGCATCCTGAAGGCCATCC-3′. The K143A mutation was made using the forward primer 5′-CGGTTACATCTATCGAGCACCAAAAGGTCTCTATATTAC-3′ and the reverse primer 5′-GTAATATAGAGACCTTTTGGTGCTCGATAGATGTAACCG-3′. The underlined bases are those changed from the wild-type sequence. After the mutagenic reaction was completed, the DNA was sequenced to confirm the presence of the desired mutation. The M15 strain of *Escherichia coli* used for protein expression was transformed with the mutated vector. The mutant enzymes was expressed and purified in a manner similar to the wild-type enzyme (*15*).

RESULTS

Fluorescence Titration. Malate is known to activate the enzyme in the direction of reductive carboxylation of pyruvate (*9*−*10*). The activation could be a result of malate binding to the active site or to an allosteric site. To determine whether malate binds to more than one site, a fluorescence titration of the malic enzyme with malate was carried out. In the absence of divalent metal ion, the active site dissociation constant for E:malate is 20 mM (*16*), while the

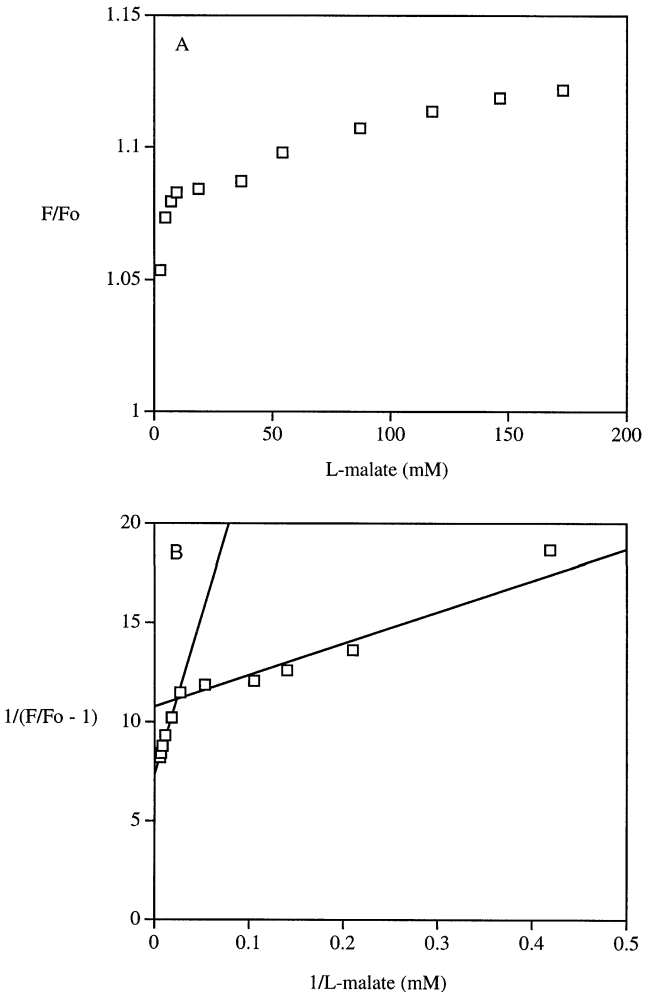

FIGURE 1: Fluorescence titration of malic enzyme. Conditions are as described in Methods. (A) Quenching, given as fluorescence in the absence (F_o) relative to that in the presence (F) of malate. Note the biphasic titration curve, resulting from malate binding to two distinct sites on enzyme with significantly different K_d values. (B) Plot of $1/(F/F_O - 1)$ against the reciprocal of malate concentration. The linear segments are from a fit of the Michaelis Menten equation to the data defining a straight line. (Although data should be fitted to a sum of two binding isotherms, the data are not well conditioned at high reactant concentration, and the low affinity K_d is undefined. However, there is more than an order of magnitude difference in the observed K_d values and the fit of the linear segments is adequate under these conditions. In agreement, the high affinity K_d obtained from the fit to a sum of two binding isotherms is 1.3 ± 0.3 mM, within error to that obtained from the linear segment (1.7 mM).)

activation constant estimated from activation in the direction of reductive carboxylation is 50 μM (*10*).

Excitation of malic enzyme at 280 nm gives an emission spectrum centered at 336 nm (data not shown). Binding of malate to the malic enzyme results in a quenching of the enzyme's intrinsic tryptophan fluorescence. The amount of fluorescence quenching measured as F/F_O, where F_o is the fluorescence of enzyme alone and F is the fluorescence of enzyme in the presence of malate, as a function of malate concentration is shown in Figure 1. A biphasic curve is obtained, and a double reciprocal plot of the data allows estimates of 1.7 and 25 mM for the two dissociation constants, in agreement with the previously reported data (*9*−*10*).[2] Data are consistent with the binding of malate to two sites, the active site and an allosteric site.

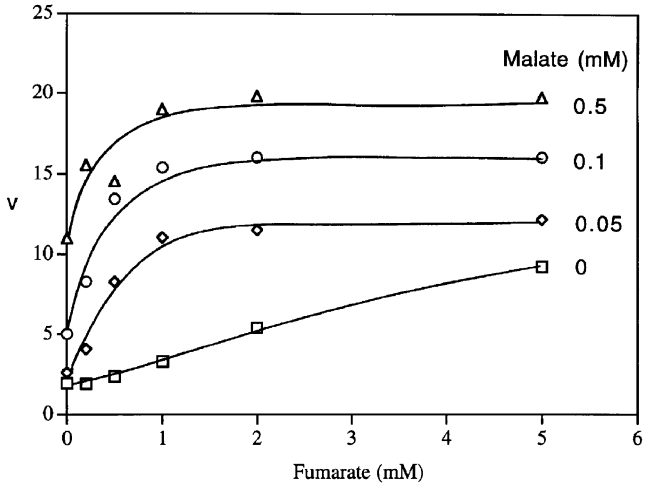

FIGURE 2: Double activation of the malic enzyme by malate and fumarate. The initial velocity was measured in the reductive carboxylation reaction direction at pH 7, 100 mM Hepes with 0.1 mM NADH, 5 mM CO_2, 1 mM Mn^{2+}, and 10 mM pyruvate. The fumarate and malate concentrations used are those indicated in the figure.

Activation in the Direction of Pyruvate Reductive Carboxylation. Both malate and fumarate activate the malic enzyme reaction (*8*−*10*). To determine whether L-malate and fumarate bind to the same activator site a double activation experiment was carried out in the reductive carboxylation direction. Under these conditions, active site binding of malate is minimal because of the presence of pyruvate. The substrate and divalent metal ion activator concentrations were fixed as discussed in Methods, and the initial rate was measured at increasing concentrations of fumarate and the experiment was then repeated at different fixed concentrations of malate (including zero) in the range where activation is observed. At each of the different L-malate concentrations used, the saturation curve for fumarate activation is hyperbolic and the maximum rate increases with increasing malate concentration, Figure 2. Data indicate there are two separate activator-binding sites, one for malate and one for fumarate. Taken together with data obtained from the fluorescence titration, three distinct sites are indicated, the active site, and two separate allosteric sites, one specific for malate and a second specific for fumarate.

The activation constants estimated for fumarate as a function of malate concentration and that estimated for malate as a function of fumarate concentration are shown in Figure 3. In both cases, the activation constant decreases as the concentration of the other effector is increased. The K_{act} for L-malate decreases to a value of about 20 μM at saturating fumarate, and the K_{act} for fumarate decreases to a value of about 100 μM at a concentration of malate that saturates the malate activator site. The data in Figure 3 indicate a synergism in the binding of the activators malate and fumarate, consistent with two separate binding sites for the two effectors. Competition for the same binding site by malate and fumarate would lead to an increase in the apparent K_{act} value for one activator as the concentration of the second activator is increased.

[2] The value of 1.7 mM is about 5-fold higher than that measured below as a result of the complete absence of active site occupancy by metal ion or reactants.

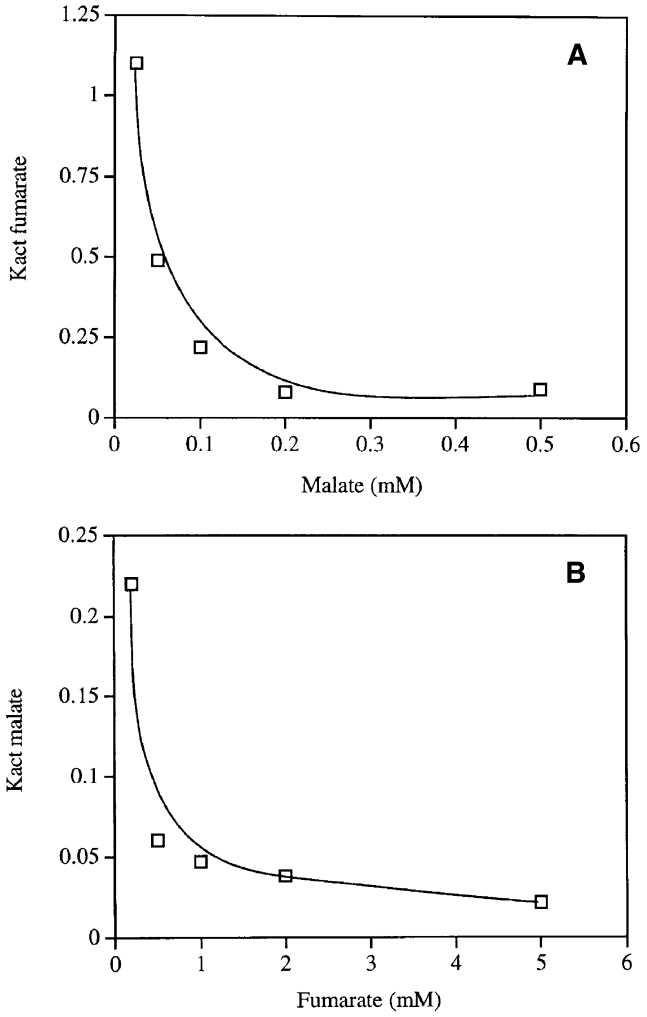

FIGURE 3: Dependence of the activation constant for one effector on the concentration of the other. (A) The K_{act} for fumarate is plotted vs L-malate concentration. The K_{act} for fumarate was calculated from curves such as those shown in Figure 2. The rate in the absence of fumarate was subtracted from each of the rates measured in the presence of fumarate and fitting the data using eq 1. The operation was then repeated at each of the different L-malate concentrations indicated. (B) The K_{act} for L-malate is plotted vs the reciprocal of fumarate concentration. K_{act} was estimated as for fumarate above.

Initial velocity patterns in the reductive carboxylation reaction direction were carried out in the absence or presence of different activating concentrations of malate or fumarate. No significant effect was observed on the maximum rate, K_{CO2}, or K_{NADH} (data not shown). Experiments were then carried out at saturating NADH and 5 mM CO_2, measuring the initial rate at varying concentrations of pyruvate and the divalent metal ion activator. In the absence of either activator the initial velocity pattern is fitted best using eq 2 for a equilibrium ordered mechanism with the metal ion binding prior to pyruvate. As the activator concentrations increase, the patterns become increasingly parallel, consequently, the intial velocity data in the presence of activators were fitted using eq 3 for a sequential mechanism to estimate both $K_{pyruvate}$ and $K_{i\ Mn}$. Plots of $K_{pyruvate}$ and $K_{i\ Mn}$ vs fumarate or malate concentration are shown in Figure 4. The value of $K_{pyruvate}$ decreases from about 30 mM in the absence of activator to a value of about 10 mM at the highest concentration of either L-malate or fumarate used. The $K_{i\ Mn}$ value also decreases from about 10 mM in the absence of activators to about 0.5 mM at the highest L-malate concentration and to about 0.05 mM at the highest fumarate concentration. In the presence of both activators, the $K_{i\ Mn}$ is less than 0.1 mM (poorly determined). The overall effect of both activators is to increase the affinity of the enzyme for pyruvate and the divalent metal ion activator, with fumarate being the most effective. In the presence of both activators, the dissociation constant for the metal ion is decreased about 2 orders of magnitude. At low fixed divalent metal ion and/or pyruvate concentrations, the presence of the either activator activates the enzyme by increasing the occupancy at the active site leading to an increase in rate.

The greatest effect of the activator would be at the lowest substrate or metal ion concentrations. Initial rates were measured at estimated physiologic concentrations of reactants and metal ion (*20*), i.e., NAD, Mg^{2+}, and malate maintained at 70 μM, 0.5 mM, and 0.2 mM, respectively. Under these conditions, the rate increases 15-fold as fumarate is increased from 0 to 2 mM, and then begins to decrease as the concentration is increased further as a result of competition between fumarate and malate at the active site (*9*). The 15-fold activation is a lower limit since the concentration of malate is sufficient to partially saturate the malate activator site.

Activation by Fumarate in the Direction of L*-Malate Oxidative Decarboxylation.* To further define the allosteric effects of fumarate and malate, initial rate studies were carried out in the direction of malate oxidative decarboxylation with malate varied. Under these conditions, the double reciprocal plot is concave upward at zero fumarate, Figure 5A. The observed nonlinearity of the double reciprocal plot at low fumarate concentrations is likely due to L-malate binding to an allosteric site and activating the reaction, increasing the affinity for malate at the active site, i.e., it reflects malate binding to two sites. In agreement with this suggestion, a plot of v vs [malate] is sigmoid, while a plot of v vs [malate]^2 is hyperbolic, Figure 5B. Once the activator site is fully occupied the double reciprocal plots become linear. Increasing the concentration of fumarate reduces the curvature and eliminates it at high fumarate concentration as a result of the increased affinity of malate for the active site. Fumarate activates the reaction by about 6-fold at the lowest L-malate concentration (0.05 mM) used, but only activates about 1.5-fold at 0.5 mM L-malate, in agreement with previous studies (*9*). Little or no activation by fumarate is observed at L-malate concentrations of 1 mM and above.

Site-Directed Mutagenesis. The crystal structure of the *Ascaris* malic enzymes indicate that R105 is an important residue for binding effector at the activator site (*14*). A sequence alignment between the *Ascaris* and human mitochondrial enzymes is shown in Figure 6. All of the residues shown to interact with fumarate in the allosteric site of the human enzyme are conserved in the site of the *Ascaris* enzyme. Thus, the R105A mutant was made and an initial velocity pattern obtained varying malate and Mg^{2+}, Figure 7. The data are fitted best using the equation for an equilibrium ordered mechanism with Mg^{2+} binding to enzyme prior to malate, qualitatively identical to the wild-type enzyme. Unlike the pattern obtained for wild-type malic enzyme, there is no evidence for deviation from linearity in the malate saturation curve, suggesting the R105A mutant may not be activated by malate. The effect of malate or

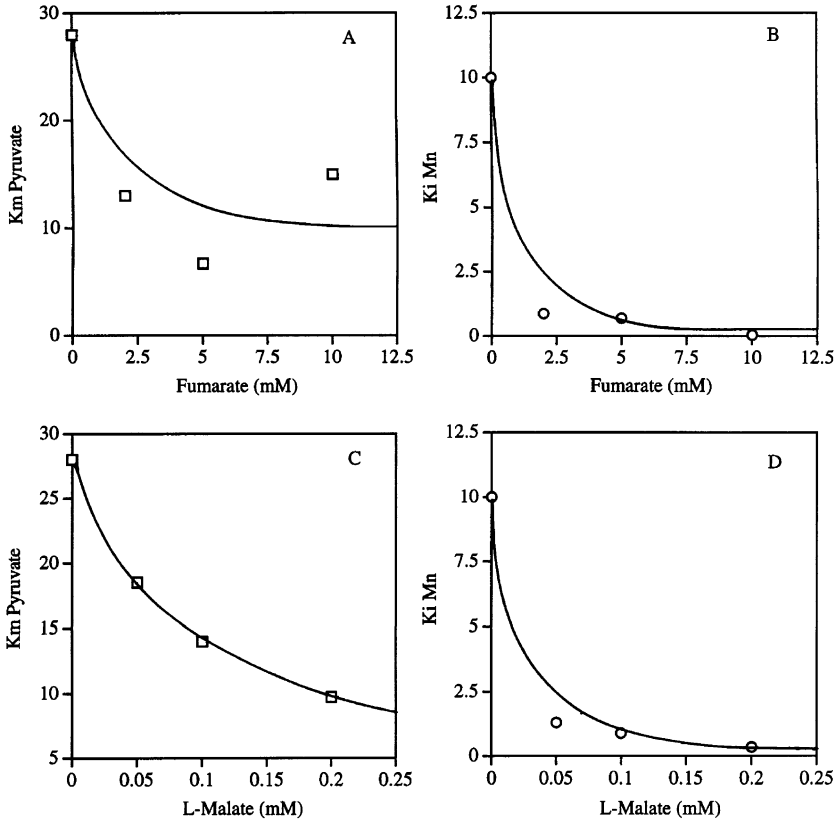

FIGURE 4: Dependence of $K_{i\ Mn}$ and $K_{pyruvate}$ on the concentration of effectors. Initial velocity patterns were obtained varying pyruvate at different fixed concentrations of Mn^{2+} at several different fixed concentrations of fumarate or L-malate. Assays were carried out at pH 7, 100 mM Hepes, with CO_2 and NADH maintained at 5 and 0.2 mM, respectively. Data were fitted using eq 3. (A) $K_{pyruvate}$ vs fumarate. (B) $K_{i\ Mn}$ vs fumarate. (C) $K_{pyruvate}$ vs L-malate. (D) $K_{i\ Mn}$ vs L-malate.

fumarate on enzyme activity is shown in Figure 8. No evidence for activation of the R105A mutant by either malate or fumarate is observed. Kinetic parameters for the R105A mutant and wild-type enzymes in the direction of oxidative decarboxylation are presented in Table 1. The K_{NAD} is increased slightly, if at all, and V is unaffected for the mutant enzyme. Thus, once the active site is saturated with substrates the wild type and the R105A mutant enzymes are equally efficient catalysts. The most significant differences between the wild type and mutant enzymes are an increase of about 6-fold in K_{malate} and 5-fold in $K_{i\ Mg}$ for R105A. The kinetic parameters for the mutant enzyme represent a less active form of the malic enzyme, while the wild-type values are for the L-malate activated enzyme since the values were obtained under conditions where the malate activator site is occupied. The values measured for the R105A mutant enzyme may reflect those of the wild-type enzyme in the direction of oxidative decarboxylation if parameters could be determined with the malate activator site unoccupied.

In addition to the residues in the allosteric site, there are other positively charged residues in a site contiguous to the allosteric site, including K143 (*12*). Therefore, a mutant enzyme was prepared in which K143 was replaced with A. Similar to the wild type enzyme, the K143A mutant of malic enzyme displays nonlinear saturation curves in the oxidative decarboxylation reaction direction (Figure 9A). However, the range of malate concentrations where the nonlinear kinetics are observed are significantly higher (0.5−10 mM) than with the wild type enzyme. The K143A mutant enzyme is also activated by fumarate (Figure 9B), but again at a significantly higher range of concentrations of fumarate than seen with wild-type enzyme. To estimate the K_{act} for fumarate for the K143A mutant enzyme a pyruvate saturation curve was done at different concentrations of fumarate and the data were fitted using eq 1 to estimate V/K at each fumarate concentration. The V/K values obtained are plotted against the fumarate concentration in Figure 10. The data in Figure 10 were fitted using eq 4.

$$y = (a + b(F/K_{act}))/(1 + F/K_{act}) \qquad (4)$$

where $y = V/K$, F is fumarate concentration, the constant a is V/K when the activator site is empty ($F = 0$), and b is V/K when the activator site is saturated ($F = \infty$). When the fumarate concentration is equal to K_{act}, V/K is equal to $1/2(a + b)$ and the fumarate activator site is half occupied. A fit of the data in Figure 10 gave a K_{act} of 26 mM for fumarate, about 10-fold higher than that obtained for the wild-type enzyme, Figure 3.

Activator Specificity. The specificity of the activator site was reported previously under conditions of saturating metal ion concentration (*9*). The activator site accommodates 4-carbon dicarboxylic acids that can attain an extended configuration. Since tartronate is bound to the activator site in the crystal strucure of *A. suum* malic enzyme (*14*), it was important to determine whether tartronate is an activator. Tartronate was varied from 0.2 to 10 mM at fixed nonsaturating concentrations of substrates in both the forward and reverse reactions, but no definitive evidence for activation by tartronate was observed (data not shown). In addition, fixing the con-

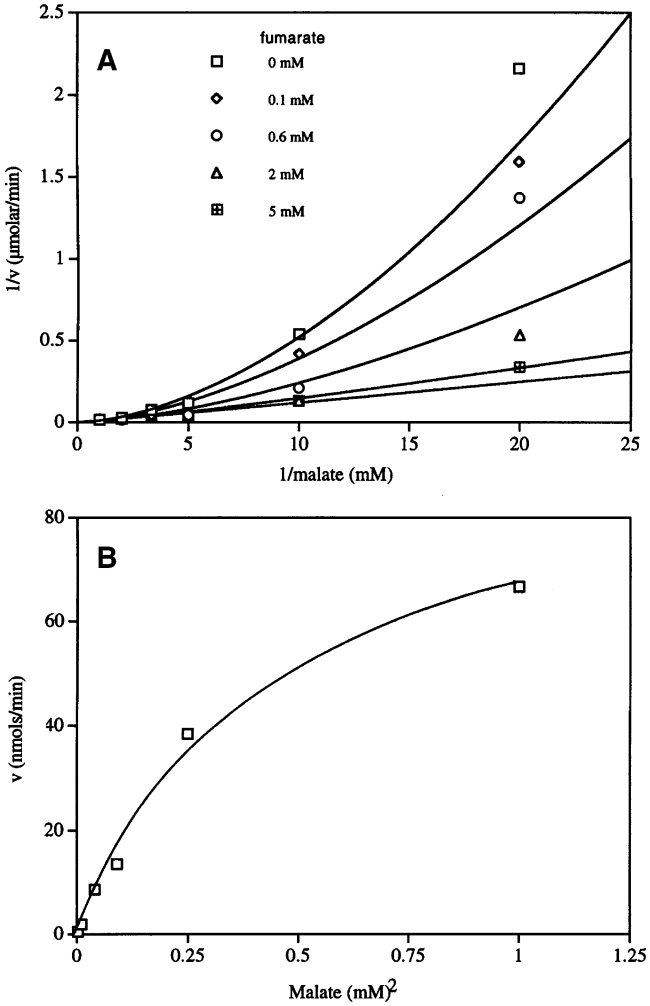

FIGURE 5: Dependence of the malate saturation curve on the concentration of fumarate. (A) Double reciprocal plot of 1/velocity vs 1/L-malate at pH 7, 100 mM Hepes, at different fixed concentrations of fumarate as indicated in the figure. The concentrations of NAD and Mg^{2+} were fixed at 1 and 30 mM, respectively. (B) A plot of v vs [malate]^2 for the curve in (A) without fumarate present.

Species	78	81	105	142,143
Ascaris suum	EQQAY**R**VITK		LQD**R**NEKL	ACQNFGYIY**RK**P
Human Mito – NADP	DV**Q** LL**R**IMRY		LQD**R**NEKL	ACQHYGLTF**RR**P
Human Mito NAD	DI**Q**A L**R**FHRN		IQD**R**NEKL	ACSQYGHIF**RR**P

FIGURE 6: Multiple sequence alignment of the *Ascaris* and human mitochondrial malic enzymes. The alignment is restricted to those areas identified as part of the fumarate binding site in the human mitochondrial NAD-malic enzyme, and a region adjacent to the fumarate site.

centration of tartronate at 1 mM greatly diminishes, 9-fold, the activation by either malate or fumarate (data not shown).

DISCUSSION

The first report of activation of the mitochondrial NAD-malic enzyme from *A. suum* was published in 1976 (*8*). The authors showed a very modest activation by fumarate under conditions in which malate is limiting. These studies were followed up in some detail in the early 90s (*9, 10*) and showed that malate was also an activator of the malic enzyme in the direction of reductive carboxylation (K_{act} = 50 μM). In addition, the authors demonstrated that activation was a result of decreasing the off-rate constant for malate from the E:NAD:Mg:malate quaternary complex. Although the earlier studies were carefully carried out, all of the kinetic data were

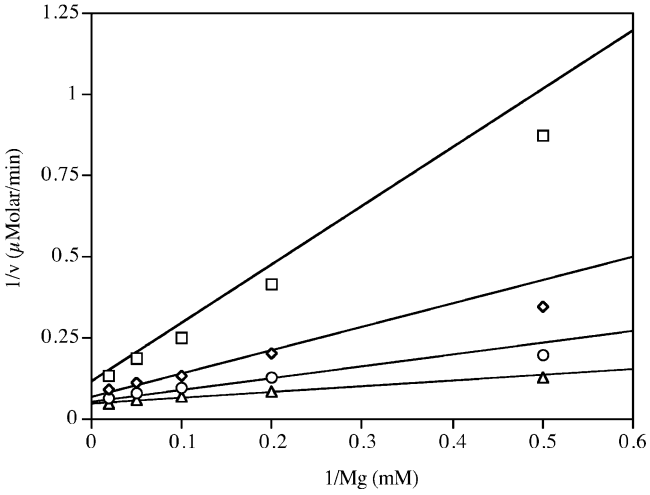

FIGURE 7: Initial velocity pattern for the R105A mutant of malic enzyme. The initial rate was measured at pH 7, 100 mM Hepes, varying Mg^{2+} at different fixed concentrations of L-malate. The NAD concentration was fixed at 1 mM. Data points are the experimentally determined values and the curves are derived from a fit of the data using eq 2.

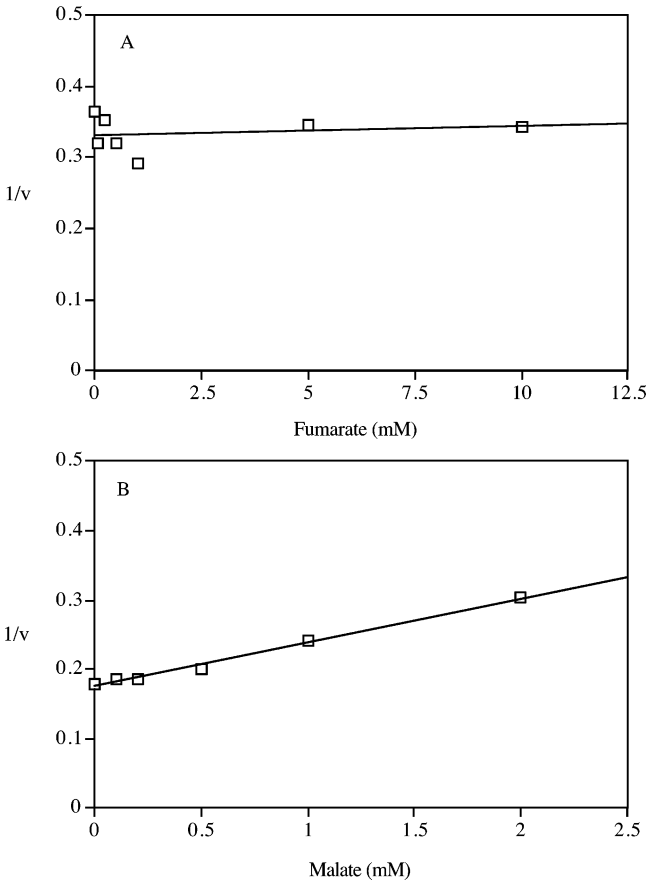

FIGURE 8: Dixon plot for fumarate and malate for the R105A mutant of malic enzyme. (A) Plot of the reciprocal of the initial rate vs fumarate concentration. Substrate concentrations are 0.5 mM L-malate, 0.5 mM NAD, and 50 mM Mg^{2+}. (B) Plot of the reciprocal of the initial rate vs malate concentration. Substrate concentrations are 20 mM pyruvate, 10 mM Mn^{2+}, 0.1 mM NADH, and 5 mM CO_2. Initial rates are measured as μM/min. All data are measured at pH 7, 100 mM Hepes.

Table 1: Comparison of Kinetic Parameters for Wild Type and R105A Mutant Enzymes.

	wild type[a]	R105A
V/E_t (s^{-1})	36[b]	33
$V/K_{malate}E_t$ ($M^{-1}\,s^{-1}$)	7×10^4	1.1×10^4
$VK_{NAD}E_t$ ($M^{-1}\,s^{-1}$)	1×10^6	4.9×10^5
$V/K_{Mg}E_t$ ($M^{-1}\,s^{-1}$)	8×10^3	1.4×10^3
K_{malate} (mM)	0.5	3.0
K_{NAD} (mM)	0.04	0.07
K_{Mg} (mM)	5	23

[a] Kinetic parameters are from (Karsten et al., 1999). [b] Errors on the parameters are all less than 20% of the value reported in the table.

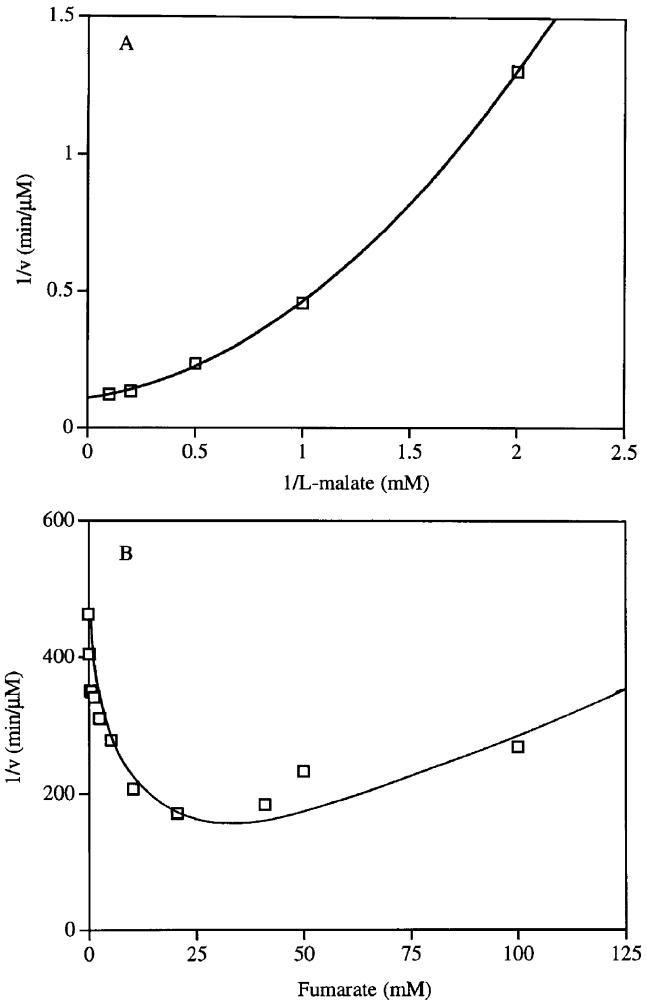

FIGURE 9: Activation of the K143A mutant of malic enzyme. (A) Reciprocal plot of 1/velocity (μM/min) vs 1/L-malate with 100 mM Hepes buffer at pH 7. NAD was fixed at 1 mM and Mg^{2+} was fixed at 20 mM. (B) A Dixon plot of 1/velocity (μM/min) vs fumarate concentration with 100 mM Hepes buffer at pH 7. NAD was fixed at 1 mM, Mg^{2+} at 160 mM, and L-malate at 1 mM.

obtained at saturating Mg^{2+} (160 mM). Below, an overview of the kinetic mechanism of activation by fumarate and malate is presented.

Do Malate and Fumarate Bind to the Same Activator Site? Because the activation constant for malate is much less than K_{malate}, it is very difficult to study malate activation in the direction of oxidative decarboxylation. Fortunately, both malate and fumarate activate in the reverse reaction direction, and it is this reaction direction that was used to probe the question of mutual exclusivity of the two activators. Double

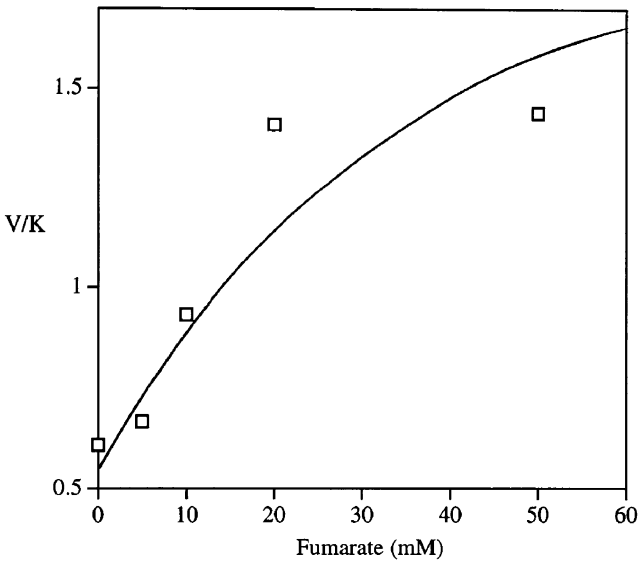

FIGURE 10: Effect of fumarate on the V/K for pyruvate for the K143A mutant. Plot of $V/K_{pyruvate}$ vs fumarate with 100 mM Hepes buffer at pH 7. NADH was fixed at 0.1 mM, CO_2 at 5 mM, and Mn^{2+} at 10 mM.

competitive activation, where the activators bind to the same site, would be expected to give a double activation pattern where the curves converge to the same maximum rate. The data shown in Figure 2, however, clearly show that activation by malate is obtained even under conditions in which fumarate is saturating with respect to its activation. Data thus indicate separate activator binding sites for malate and fumarate. Quantitative analysis of the data are in agreement with this suggestion. The activation constant for fumarate decreases as the concentration of malate increases, and increasing fumarate affects the malate activation constant in an identical manner. The synergistic binding of the two effectors can only be explained by the presence of separate, yet interactive activator binding sites. These sites are separate from the active site.

Theory. A schematic depiction of the kinetic mechanism of activation is shown in Scheme 1. In Scheme 1, E represents the E:NAD complex with CO_2 fixed, while A represents Mn^{2+} and pyruvate, which are treated simultaneously here for simplicity. Since the maximum rate is unaffected by the presence of the activators, the rate of production of products from all quaternary complexes (E:NAD:M:malate, (malate)E:NAD:M:malate, (fumarate)-E:NAD:M:malate, and (fumarate)(malate)E:NAD:M:malate) are assumed to be identical. A rate equation derived based on the model presented in Scheme 1 using the rapid equilibrium assumption of Cha (*25*) is given as eq 5

$$\frac{v}{E_t} = \frac{k_{cat}\left(\frac{A}{K_a} + \frac{AI}{\alpha K_a K_i} + \frac{AJ}{\beta K_a K_j} + \frac{AIJ}{\delta\gamma K_a K_i K_j}\right)}{1 + \frac{A}{K_a} + \frac{I}{K_i} + \frac{J}{K_j} + \frac{AI}{\alpha K_a K_i} + \frac{AJ}{\beta K_a K_j} + \frac{IJ}{\gamma K_i K_j} + \frac{AIJ}{\delta\gamma K_a K_i K_j}} \quad (5)$$

In eq 5, A, I, and J represent malate as a substrate, malate as an activator and fumarate, respectively, k_{cat} is the rate constant for product formation from the respective Michaelis constants defined above, and the dissociation constants are as defined in the scheme. The Greek symbols are interaction coefficients that will have values less than 1 in the case of

Scheme 1: Schematic Mechanism for Interaction of Malate at the Active Site, and Malate and Fumarate at Different Allosteric Sites[a]

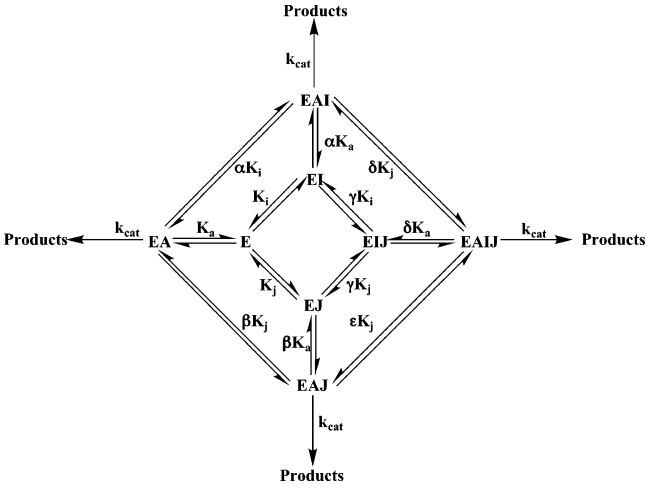

[a] Since V_{max} is unaffected, all EA complexes are converted to product with the same rate constant, k_{cat}. All other terms are defined in the text.

synergism of binding. The limits of the above equation are as follows:

$$\mathrm{I,J} \xrightarrow[\text{lim}]{} 0 \qquad \frac{v}{E_t} = \frac{k_{cat}\mathrm{A}}{K_a + \mathrm{A}} \tag{6}$$

$$\mathrm{I} \xrightarrow[\text{lim}]{} 0;\ J \xrightarrow[\text{lim}]{} \infty \qquad \frac{v}{E_t} = \frac{k_{cat}\mathrm{A}}{\beta K_a + \mathrm{A}} \tag{7}$$

$$\mathrm{J} \xrightarrow[\text{lim}]{} 0;\ \mathrm{I} \xrightarrow[\text{lim}]{} \infty \qquad \frac{v}{E_t} = \frac{k_{cat}\mathrm{A}}{\alpha K_a + \mathrm{A}} \tag{8}$$

$$\mathrm{I,J} \xrightarrow[\text{lim}]{} \infty \qquad \frac{v}{E_t} = \frac{k_{cat}\mathrm{A}}{\delta K_a + \mathbf{A}} \tag{9}$$

and with $\mathrm{A} = K_a$, eq 5 reduces to eq 10, which reflects the experiment shown in Figure 2.

$$\frac{v}{E_t} = \frac{k_{cat}\left(1 + \dfrac{\mathrm{I}}{\alpha K_i} + \dfrac{\mathrm{J}}{\beta K_j} + \dfrac{\mathrm{IJ}}{\delta\gamma K_i K_j}\right)}{\left(2 + \dfrac{\mathrm{I}}{K_i} + \dfrac{\mathrm{J}}{K_j} + \dfrac{\mathrm{IJ}}{\gamma K_i K_j}\right) + \left(\dfrac{I}{\alpha K_i} + \dfrac{\mathrm{J}}{\beta K_j} + \dfrac{\mathrm{IJ}}{\delta\gamma K_i K_j}\right)} \tag{10}$$

The limits of eq 10 are as follows:

$$\mathrm{I} \xrightarrow[\text{lim}]{} 0\ \frac{v}{E_t} = \frac{k_{cat}\left(1 + \dfrac{\mathrm{J}}{\beta K_j}\right)}{2 + \left(\dfrac{\mathrm{J}}{K_j}\right)\left(1 + \dfrac{1}{\beta}\right)} \tag{11}$$

$$\mathrm{J} \xrightarrow[\text{lim}]{} 0\ \frac{v}{E_t} = \frac{k_{cat}\left(1 + \dfrac{\mathrm{I}}{\alpha K_i}\right)}{2 + \left(\dfrac{\mathrm{I}}{K_i}\right)\left(1 + \dfrac{1}{\alpha}\right)} \tag{12}$$

and thus experiments carried out under the above conditions allow estimates of the kinetic parameters and interaction coefficients.

In the present case, data are analyzed for the reverse reaction to alleviate the necessity of considering allosteric site combination of malate under conditions where malate is used as a substrate. In addition, the change in the $K_{i\ Mn}$ is the most sensitive indicator of interaction between active and allosteric sites, and will be used as K_a in the above rate equations. On the basis of the above mechanism and rate equations, the following can be discerned. From the data in Figure 4, the $K_{i\ Mn}$ is 10 mM in the absence of effectors, and decreases to 0.5 mM in the presence of saturating malate and to 0.05 mM in the presence of saturating fumarate. Values of α and β, eqs 11 and 12, are about 0.05 and 0.005, respectively, and fumarate is a more potent effector than is malate. Values for K_i and K_j are obtained from Figure 3; the concentrations of pyruvate and Mn^{2+} are maintained at below saturation in these experiments and the values for K_i and K_j for malate and fumarate are those obtained at zero concentration of the other effector. Thus, K_i and K_j are 0.3 and 2.5 mM, respectively, and αK_i and βK_j are both about 0.01 mM, respectively. Data in Figure 3 allow an estimate of γ, the interaction coefficient between malate and fumarate. The value of K_i at saturating fumarate is 0.02 mM, while K_j is 0.15 mM at saturating malate, giving values of 0.067 (0.02/0.3) and 0.06 (0.15/2.5), respectively. Finally, an estimate for δ is obtained from the ratio of the values of $K_{i\ Mn}$ at zero effector concentration and at saturating concentration of both effectors. The $K_{i\ Mn}$ is 10 mM in the absence of effectors, and <0.1 mM in the presence of both effectors at saturating concentrations, giving an estimate of <0.01 for δ. Since the value for δ is close to the value of β, the maximum activation can only be achieved by fumarate alone, or with some combination of malate and fumarate binding to their allosteric sites.

The coefficient values defined above are equivalent to the reciprocal of the *Q* values defined by Reinhart (*26*), and they can be used to estimate the interaction free energy between sites. The free energy of interaction between the active site and the malate allosteric binding site is determined from $\Delta G^{\circ\prime} = -RT\ln(1/\alpha) = -1.8$ kcal/mol. Likewise, values for interaction between the active site and the fumarate allosteric binding site is -3 kcal/mol, and that for interaction between the two allosteric sites is -1.7 kcal/mol. As stated above, the interaction between the active site and the fumarate allosteric site is the strongest.

What Steps Along the Reaction Pathway Are Affected by Fumarate and Malate? Initial velocity patterns obtained as a function of increasing concentrations of malate, fumarate, or both in the direction of reductive carboxylation exhibit no, or very little, change in K_{NAD}, but substantial changes in $K_{pyruvate}$ and the dissociation constant for the metal ion, Mn^{2+}. Thus, the presence of either malate or fumarate bound to their activator site must produce a decrease in the off-rate constants for metal ion and pyruvate at the active site. Similar changes in the dissociation constant for Mg^{2+} and K_{malate} are observed in the direction of oxidative decarboxylation. The greatest effect on the off-rate constants for metal ion and substrate is observed at saturating concentrations of both effectors at the activator sites. This is, in fact, predicted by the data in Figure 4.

The effectors do not alter the rate constant for the catalytic steps. How then can one rationalize the activation of malic enzyme in both reaction directions? Since the effectors decrease the off-rate constants for malate and pyruvate why

is inhibition not observed in either reaction direction? The rate-limiting steps in the direction of oxidative decarboxylation are a conformational change in the E:NAD:Mg complex (*21*), hydride transfer, and decarboxylation (*22*−*23*). The off-rate constant for pyruvate must then be much greater than k_{cat}, enough so that even with the decrease in the off-rate constant for pyruvate in the presence of effectors, it is still greater than the slow steps in the forward reaction direction. In the reverse reaction direction, the off-rate constant for malate must likewise be much greater than the rate of carboxylation to give the oxalacetate intermediate.

One of the kinetic Haldane relationships for the random mechanism catalyzed by malic enzyme is given in eq 13.

$$K_{eq} = \frac{(V/K_{pyruvate})(K_{i\ NADH})(K_{i\ CO2})(K_{i\ Mn})}{(V/K_{malate})(K_{i\ NAD})(K_{i\ Mn})} \quad (13)$$

It would be expected that the $K_{i\ Mn}$ would be affected equally in both reaction directions, and in agreement, the limiting value of the metal ion dissociation constant is identical in both reaction directions under conditions in which both effectors are saturating. There is no effect of the activators on the dissociation constants for NAD or NADH, and likewise no effect on the parameters for CO_2. Since the value of K_{eq} must be the same in the absence and presence of effectors the changes in K_{malate} and $K_{pyruvate}$ must be identical.

On the basis of the relative values of K_{malate} and $K_{act\ malate}$ in the direction of oxidative decarboxylation, the malic enzyme is activated to some extent in the case of almost all of the studies that have been published previously.

Reinterpretation of Previous Data. Previously published data now make sense in view of the mechanism presented above. Pre-steady-state kinetic studies have been carried out mixing enzyme alone with NAD, Mg^{2+}, and malate (*21*). Under these conditions, a lag in the time course is observed with a rate constant of 40 s^{-1}. No change in the lag time is observed when enzyme is preincubated with NAD prior to mixing with Mg^{2+} and malate, but a 4-fold increase in the lag rate constant is obtained when enzyme is preincubated with Mg^{2+} prior to mixing. Preincubation with Mg^{2+} and malate (or fumarate), however, eliminates the lag completely. Data likely indicate slow activation by Mg^{2+} and malate in the absence of preincubation, and complete activation upon preincubation with the metal ion and activators.

The pH profiles for malic enzyme have been measured in the direction of oxidative decarboxylation (*24*). The *V/K* pH−rate profiles for malate and NAD exhibit p*K* values of about 5 and 9, reflecting the general base and general acid in the reaction; the V/K_{malate} profile also exhibits the p*K* for the β-carboxylate of malate at pH 4.9. The *V* profile, on the other hand is asymmetric, and is pH independent of the basic side, but shows a p*K* of 5 on the acid side. Using thioNAD as a slow (<10% k_{cat}) alternative dinucleotide substrate, the p*K* of 5 is not observed. Data were interpreted in terms of a pH-dependent conformation change in the E:NAD complex. At pH 4.4, where the chemical steps have decreased in rate by greater than 10-fold compared to neutral pH, no lag is observed in the pre-steady-state time course, i.e., the rate of the conformational change no longer limits at this low pH. We propose that the pH dependence of the conformation change reflects the pH dependence of malate binding to its allosteric site. Consistent with the proposal, the p*K* observed in the *V* profile is identical to that of the β-carboxylate of malate.

Location of the Allosteric Sites and Transmission of the Allosteric Signal. An allosteric site with tartronate bound in the *A. suum* malic enzyme was located at the dimer interface (*14*). The site is homologous to the fumarate binding site identified recently in the human mitochondrial NAD-malic enzyme (*13*). It is thus likely that the site identified is the fumarate allosteric binding site with tartronate bound. Although tartronate binds to the allosteric site, it does not activate (see above). As pointed out above, the interaction between tartronate and the residues in the allosteric site of the *Ascaris* enzyme differ from those between fumarate and the same residues in the allosteric site of the human enzyme.

In agreement with the site being an activator site, the R105A mutant enzyme is no longer activated by fumarate. It has also been shown that the R91T mutation in the human enzyme (R91 is the homologue of R105 in the *Ascaris* enzyme) gives the same effect (*13*). In addition, however, the mutation also eliminates activation by malate in the *Ascaris* enzyme, consistent with the interaction between the two sites for activation (see above). The fumarate and malate sites may be close or adjacent to one another so that mutation of R105 may disrupt binding of both activators. Alternatively, malate could conceivably bind to the R105A mutant enzyme, but the mutation may disrupt transmission of the signal through the protein to the active site.

A possible location for the malate site is suggested by the behavior of the K143A mutant enzyme. Consistent with this suggestion, the activation constants for malate and fumarate increase into the millimolar range, compared to those measured in the micromolar range for the wild type enzyme. The activation constant for fumarate increases almost 3 orders of magnitude in the K143A mutant enzyme. Lysine-143 is located in a positively charged pocket adjacent to the fumarate site and can communicate with the fumarate site via backbone interactions between the sites (*14*). Whether this is actually the site will have to await further mechanistic and structural studies.

REFERENCES

1. Saz, H. J. (1971) *Am. Zool. 11*, 125−135.
2. Saz, H. J., and Lescure, O. L. (1969) *Comp. Biochem. Physiol. 30*, 49−60.
3. Papa, S., Cheah, K. S., Rasmussen, H. N., Lee, I. Y., and Chance, B. (1970) *Eur. J. Biochem. 12*, 540−543.
4. Fodge, D. W., Gracy, R. W., and Harris, B. G. (1972) *Biochim. Biophys. Acta 268*, 271−284.
5. Kmetec, E., and Bueding, E. (1961) *J. Biol. Chem. 236*, 584−591.
6. Seidman, I., and Entner, N. (1961) *J. Biol. Chem. 236*, 915−919.
7. Rew, R. S., and Saz, H. J. (1974) *J. Biol. Chem. 63*, 125−135.
8. Landsperger, W. J., and Harris, B. G. (1976) *J. Biol. Chem. 251*, 3599−3602.
9. Lai, C.-J., Harris, B. G., and Cook, P. F. (1992) *Arch. Biochem. Biophys. 299*, 214−219.
10. Mallick, S., Harris, B. G., and Cook, P. F. (1991) *J. Biol. Chem. 266*, 2732−2738.
11. Xu, Y., Bhargava, G., Wu, H., Loeber, G., and Tong, L (1999) *Structure 7*, 877−889.

12. Coleman, D. E., Rao, G. S., Goldsmith, E. J., Cook, P. F., and Harris, B. G. (2002) *Biochemistry 41*, 6928−6938.
13. Yang, Z., Lanks, C. W., and Tong, L. (2002) *Structure 10*, 951−960.
14. Rao, G. S. J., Coleman, D. E., Karsten, W. E., Cook, P. F., and Harris, B. G. (2003) *J. Biol. Chem. 278*, (in press).
15. Karsten, W. E., Chooback, L., Liu, D., Hwang, C.-C., Lynch, C., and Cook P. F. (1999) *Biochemistry 38*, 10527−10532.
16. Park, S.-H., Kiick, D. M., Harris, B. G., and Cook, P. F. (1984) *Biochemistry 23*, 5446−5453.
17. Martell, A. E., and Smith, R. M. (1977) *Critical Stability Constants*, Vol 3, Plenum Press, New York.
18. Martell, A. E., and Smith, R. M. (1982) *Critical Stability Constants*, Vol 5, Plenum Press, New York.
19. Cleland, W. W. (1979) *Methods Enzymol. 63*, 103−108.
20. Barrett, J., and Beis, I. (1973) *Comp. Biochem. Physiol. B 44*, 751−761.
21. Rajapaksa, R., Abu-Soud, H., Rauschel, F. M., Harris, B. G., and Cook, P. F. (1993) *Biochemistry 32*, 1928−1934.
22. Weiss, P. M., Gavva, S. R., Harris, B. G., Urbauer, J. C., Cleland, W. W., and Cook P. F. (1991) *Biochemistry 30*, 5755−5763.
23. Karsten, W. E., and Cook, P. F. (1994) *Biochemistry 33*, 2096−2103.
24. Kiick, D. M., Harris, B. G., and Cook, P. F. (1986) *Biochemistry 25*, 227−236.
25. Cha, S. (1968) *J. Biol. Chem. 243*, 820−825.
26. Reinhart, G. D. (1983) *Arch. Biochem. Biophys. 224*, 389−395.

BI034101W